Organelle Transport along Microtubules in *Xenopus* Melanophores: Evidence for Cooperation between Multiple Motors

Valeria Levi,* Anna S. Serpinskaya,† Enrico Gratton,* and Vladimir Gelfand†
*Laboratory for Fluorescence Dynamics, University of Illinois at Urbana-Champaign, Urbana, Illinois; and
†Department of Cell and Molecular Biology, Feinberg School of Medicine, Northwestern University, Chicago, Illinois

ABSTRACT *Xenopus* melanophores have pigment organelles or melanosomes which, in response to hormones, disperse in the cytoplasm or aggregate in the perinuclear region. Melanosomes are transported by microtubule motors, kinesin-2 and cytoplasmic dynein, and an actin motor, myosin-V. We explored the regulation of melanosome transport along microtubules in vivo by using a new fast-tracking routine, which determines the melanosome position every 10 ms with 2-nm precision. The velocity distribution of melanosomes transported by cytoplasmic dynein or kinesin-2 under conditions of aggregation and dispersion presented several peaks and could not be fit with a single Gaussian function. We postulated that the melanosome velocity depends linearly on the number of active motors. According to this model, one to three dynein molecules transport each melanosome in the minus-end direction. The transport in the plus-end direction is mainly driven by one to two copies of kinesin-2. The number of dyneins transporting a melanosome increases during aggregation, whereas the number of active kinesin-2 stays the same during aggregation and dispersion. Thus, the number of active dynein molecules regulates the net direction of melanosome transport. The model also shows that multiple motors of the same polarity cooperate during the melanosome transport, whereas motors of opposite polarity do not compete.

INTRODUCTION

Organization of the cytoplasm of eukaryotic cells depends on the function of molecular motors that move organelles and other cellular cargoes along microtubules and microfilaments to their correct destination in the cytoplasm. A large number of molecular motors belonging to the kinesin, dynein, and myosin superfamilies have been identified using genetic and cell biological techniques and the atomic structures of some of these motors were solved by x-ray crystallography (see references in Howard (1)).

The common core structure of most of these motors consists of two motor domains connected by a stalk to a globular tail that binds to the cargo. The motor domains attach to the microtubules in a coordinate manner and undergo conformational changes, driven by ATP hydrolysis, which propel the motor molecule (for recent reviews, see Welte (2) and Vale (3)). For some members of the myosin and kinesin superfamilies, it has been shown that the motion follows a hand-over-hand mechanism in which both heads alternate in the lead while moving along the cytoskeleton element (4–6). The biophysical properties of molecular motors have been extensively analyzed in the past several years and, in many cases, we know how the energy provided by ATP hydrolysis is coupled to the mechanical work exerted by the motor moving along actin filaments or microtubules (see, for example, Schnitzer et al. (7)).

Despite detailed knowledge of the structure and the working cycle of many individual motors in vitro, little is known about the molecular mechanisms involved in the precise spatial and temporal control of the motors during organelle transport. The presence of motors of the opposite polarity on the surface of the cargo raises the question of their coordination. In the absence of such coordination, different motors would be involved in a tug-of-war, thus preventing effective transport. Indeed, several recent studies using a number of biological models demonstrated that plus- and minus-end-directed microtubule motors are not involved in a tug-of-war and do not work against each other, although molecular mechanisms of such coordination still remained a mystery (8). Even less is known about the contribution of multiple molecules of motors of the same polarity to a net movement of cargo. One recent study suggests that multiple kinesins or multiple dyneins on the surface of peroxisomes could work in a cooperative fashion (9), but it is not clear how general is this observation or what is the mechanism of such cooperation.

Questions of motor cooperativity can be conveniently addressed using pigment cells or melanophores, cells that have been successfully used in the past to study the mechanism and regulation of intracellular transport (reviewed in Nascimento et al. (10)). The major physiological task of these cells is to move pigment organelles called melanosomes in the cytoplasm, allowing animals to display color change. *Xenopus* melanophores have melanosomes filled with the black pigment melanin, and therefore these organelles can be easily imaged and discriminated from other cellular components using brightfield transmission light microscopy without the need of any contrast generation technique or the use of fluorescent probes.

Submitted June 2, 2005, and accepted for publication September 20, 2005.

Address reprint requests to Enrico Gratton, Laboratory for Fluorescence Dynamics, University of Illinois at Urbana-Champaign, 1110 West Green St., Urbana, IL 61801. Tel.: 217-244-5620; Fax: 217-244-7187; E-mail: enrico@scs.uiuc.edu.

0006-3495/06/01/318/10 $2.00

doi: 10.1529/biophysj.105.067843

Pigment organelles can be distributed in the cells in two different configurations—either aggregated in the perinuclear region or homogeneously dispersed in the cytoplasm. The transport of pigment organelles during aggregation and dispersion is regulated by signaling cascades initiated by the binding of specific hormones to cell-surface receptors, which results in the modulation of cAMP concentrations (11,12). Therefore, one can stimulate melanosome movement toward or away from the cell center by using appropriate hormones to decrease or increase, respectively, the concentration of cAMP in the cytoplasm.

Furthermore, melanosome transport in *Xenopus* melanophores is well characterized in terms of molecular motors participating in the movement. Pigment dispersion requires the plus-end-directed microtubule motor kinesin-2 (13) and the actin motor myosin-V (14), whereas aggregation is powered by the minus-end-directed motor cytoplasmic dynein (15). The net movement of melanosomes results from the combined action of these three motors. It is possible to eliminate the contribution of myosin-V to melanosome movement by depolymerizing actin filaments by treating the cells with latrunculin B. The remaining movement is entirely microtubule-dependent and, therefore, latrunculin-treated cells can be used to study the contribution of microtubule motors cytoplasmic dynein and kinesin-2 to the organelle transport without the contribution of the second transport system.

In this study, we used a new method of precise tracking and rapid image acquisition to compare the movement of individual melanosomes along microtubules in latrunculin-treated cells stimulated for either dispersion with the melanocyte-stimulating hormone (MSH) or aggregation with melatonin. Analysis of these data demonstrated that the velocity of melanosomes along microtubules does not follow a single Gaussian function but displays several peaks. Such a distribution can be explained by a model that considers that a small number of molecules of the plus- or minus-end motors transport each organelle away or toward the cell center, respectively. Comparison of the velocity distributions of melanosomes moving in the minus and plus directions demonstrates that the average number of active dynein molecules transporting an individual organelle increases during aggregation. In contrast, the average number of active kinesin-2 molecules per melanosome remains the same during dispersion and aggregation. Thus, we postulate that the movement of melanosomes along microtubules is regulated by activation of dynein molecules on the melanosome surface, whereas the transport mediated by kinesin-2 is not regulated.

MATERIALS AND METHODS

Cell culture and sample preparation for imaging

Immortalized *Xenopus* laevis melanophores were cultured as described (16). To track the movement of individual organelles, the number of melanosomes in the cell was reduced by treatment with phenylthiourea (17).

For microscopy measurements, the cells were grown for 2 days on 25-mm round polylysine-coated coverslips placed into 35-mm plates in 2.5 ml of the medium. Before observation, the coverslips were washed in serum-free 70% L-15 medium and mounted in a custom-made chamber specially designed for the microscope. The cells were treated with 10 μM latrunculin B (Biomol International, Plymouth Meeting, PA) for at least 30 min to depolymerize actin filaments. The cells were stimulated for aggregation or dispersion with 10 nM melatonin or 100 nM MSH, respectively. The samples were observed between 5 and 15 min after stimulation. All the measurements were performed at 21°C.

Generation of melanophore cell line with EGFP-labeled microtubules

To analyze microtubule distribution and organelle movement in the same cell, we have selected a cell line of melanophores permanently transfected with enhanced green fluorescent protein (EGFP)-tagged XTP, a *Xenopus* homolog of tau protein (18). XTP cDNA (a kind gift from Dr. Ole Olesen, Curix Biotech, Copenhagen, Denmark) was cut from pET5-XTP plasmid using *Eco*RI and then cloned into the multiple cloning site of pEGFP-C1 vector (BD Biosciences, Palo Alto, CA). Melanophores were transfected with EGFP-XTP construct, and 48 h later all microtubules in the transfected cells were labeled with EGFP. Transfected cells were selected using G418 (0.2 mg/ml) and subcloned twice. Clones showing a microtubule-specific pattern of labeling in every cell were selected and used as a stable line in the experiments. Staining with the tubulin antibody DM1 alpha and a rhodamine-labeled secondary antibody revealed a normal microtubule distribution and demonstrated that every microtubule in the cells was homogeneously labeled by EGFP-XTP (not shown). Expression of EGFP-XTP did not affect movement of melanosomes and had no effect on melanosome dispersion and aggregation by MSH and melatonin, respectively. The rate of movement of melanosomes on microtubules was not affected by EGFP-XTP expression. Therefore we could use melanophores stably expressing EGFP-XTP for simultaneous visualization of microtubules and melanosomes in live cells.

Microscope setup

The tracking experiments using the pattern recognition routine were carried out in an Olympus IX70 microscope using a 60× water-immersion objective (numerical aperture = 1.2) under illumination with a tungsten-halogen lamp. A cMOS camera (Pixelink, Ottawa, Ontario, Canada) was attached to the video port of the microscope for imaging the cells. The movies were registered at a speed of 100 frames/s except as indicated.

Two-photon microscopy experiments were carried out using an Olympus IX70 microscope, described previously (19). The excitation source was a mode-locked titanium-sapphire laser (Mira 900, Coherent, Palo Alto, CA) pumped by an argon ion laser (Innova 300, Coherent) and tuned at 915 nm, except when indicated. The average power at the sample was ~1 mW. The light is directed into the microscope by two galvomotor-driven scanning mirrors (Cambridge Technologies, Watertown, MA) through a scanning lens. The laser light is reflected with a low-pass dichroic mirror (transmission from 370 to 630 nm, Chroma Technology, Brattleboro, VT) and focused on the sample with a 63× oil-immersion plan apochromat objective (numerical aperture = 1.4). Fluorescence emission is collected by the objective and passes through a dichroic and short-pass filter to eliminate any reflected excitation light. It then exits the microscope to the detector (Hamamatsu H7422P-40 photomultiplier tube) on the side port. The output of this unit is amplified and passed through a discriminator (PX01 Photon Counting Electronics, ISS, Champaign, IL). Photons were counted with a data acquisition card (ISS).

The experiments are controlled by a custom-made data acquisition program (SimFCS, Laboratory for Fluorescence Dynamics, Champaign, IL). This program, which also contains the tools used for trajectory analysis, can be downloaded from the Laboratory for Fluorescence Dynamics website (www.lfd.uiuc.edu).

Pattern-recognition algorithm for tracking melanosomes

To start the tracking routine, the program displays the first frame of the image stack under analysis. The operator chooses the target melanosome by simply clicking on top of its image. Doing so, the program sets the initial coordinates of the melanosome and generates an intensity pattern that consists of the average intensity obtained from the first 10 frames of a region containing the melanosome image. Generally, the image size of the pattern is 12×12 pixels; however, the operator can select smaller or larger areas. This pattern is stored in the computer memory to be used during the calculation of the melanosome position through the image stack. Since the pattern contains all the details of the intensity profile of the particular melanosome and the background, it would fit almost perfectly the intensity profile of the organelle in the successive frames, if it is not moving perpendicular to the focal plane. The difference between the pattern and the melanosome image will be given by the shot noise of each individual pixel of the image.

To calculate the melanosome position in the next frame, the algorithm compares the intensity distributions of the pattern and five areas of the frame. These areas have the same size as the pattern and their positions are the following: one is exactly centered at the coordinates determined for the melanosome in the previous frame, two are located n pixels to the left and right of the center area, and two are positioned n pixels above and below the center area. In the experiments presented in this work, $n = 1$, however, this number can be adjusted by the operator.

For each of these areas, the weighted deviation (δ) is calculated as follows:

$$\delta = \sum_{i,j} \sqrt{\left(I_{image}(i,j) - I_{pattern}(i,j) - B\right)^2} \times w(i,j), \qquad (1)$$

where $I(i,j)$ is the intensity at position (i,j), B is the difference between the average backgrounds of the local image and the pattern, and $w(i,j)$ is the weighting factor that attributes more weight to points with higher contrast. This last parameter is calculated as follows:

$$w(i,j) = \sqrt{\left(I_{pattern}(i,j) - I_{border}\right)^2}, \qquad (2)$$

where I_{border} represents the average intensity at the border of the pattern.

The values of δ obtained for the three areas in the x (horizontal) and y (vertical) directions are interpolated with parabolic functions. From the interpolations, a minimum value of δ can be determined in the x and y directions. Then, the center area is repositioned to the new coordinates and the minimization routine is repeated as explained until the particle position is determined with a given tolerance, typically 1/100 of a pixel. Since the minimum of the parabolas can be located at fractional values of a pixel, the intensity of the image needs to be interpolated at the overlapping positions; this operation is done with a bilinear interpolation.

Melanosome tracking using the two-photon microscope

The tracking routine used to follow the melanosomes was that described by Levi et al. (19), with the exception that the particle motion was followed in two dimensions instead of three dimensions. This method has 20-nm precision and a time resolution of 32 ms.

Calculation of melanosome velocity

Each of the trajectories is first carefully observed and divided into fragments corresponding to motion toward the minus or plus end of the microtubules or oscillations at an approximately same position. These last fragments are not considered in the further analysis. The melanosome is considered to be moving in the minus or plus directions when >200 contiguous points of the trajectory present the same general direction, despite the small noise obtained from point to point; it is considered to be oscillating in the same position if this criterion is not fitted. If the melanosome is moving but the direction is uncertain, the fragment is also excluded from the further analysis.

After this initial classification, a plot of distance along the trajectory from the initial point as a function of time is constructed for each of the minus or plus selected fragments of the trajectory. This local trajectory is generally rectilinear, although at an angle with respect to the microscope coordinates. For the analysis, it is unimportant whether or not the trajectory is rectilinear provided that it is not changing abruptly.

Each of these distance plots is further divided in segments of 40–80 points and a linear equation is fit to determine the local velocity in the segment. The fitting of the linear equation in each segment is observed and the segment velocity is included in the statistics if the value of r^2 is $\geq$0.98.

If the fitting is not adequate due to a sudden change in velocity in the middle of a given segment, we further divide the fragment under analysis into subfragments (one before and one after the change in velocity) and repeat the segmentation in each of the subfragments. Fig. 1 represents schematically the procedure to determine velocities applied to a trajectory obtained after stimulating the cell for aggregation. In this example, we calculated the velocity of the melanosome during a minus-end run. As can be observed, the residuals obtained from the analysis (Fig. 1 *B*, *bottom*) are within 40 nm and were homogeneous along the run, showing that the fit was highly satisfactory.

Data analysis

To select the model that best describes the experimental data, we calculated the Akaike index (AIC) as follows (20):

$$\mathrm{AIC} = n_D \times \ln\left(s_{min}\right) + 2 \times n_P \qquad (3)$$

where S_{min} is the sum of the square deviations between the experimental data and the model predictions and n_D and n_p are the number of data points and parameters, respectively. The best model was chosen as the one that gives the least biased fit and the lowest AIC.

RESULTS

Performance of the tracking by the pattern-recognition routine

To check the performance of the tracking method, we mounted a nanometric stage on the microscope (Nano-Bio 2 (Mad City Labs, Madison, WI), with 0.7 nm position accuracy, used in closed-loop scanning mode). We placed a slide with a dried suspension of 500-nm-diameter polystyrene microspheres (Molecular Probes, Eugene, OR) on top of the stage and moved the slide in steps of 10–50 nm. Fig. 2 shows the trajectory recovered for one of the microspheres moving in steps of 10 nm with a time interval between steps of 100 ms. The recovered step size was linearly related to the input step size, with a slope of 1.04 ± 0.04 (Fig. 2, *inset*). The resolution of the method—calculated as the standard deviation in the position of a fixed microsphere in a movie of 20 frames acquired at 100 frames/s—was better than 2 nm.

We also calculated the signal/noise (S/N) ratios on inverted brightfield images of melanosomes in cells and fixed beads and verified that the S/N ratio of melanosomes is 50% higher than that of the beads. Thus, the performance of the method should be equally good when tracking melanosomes.

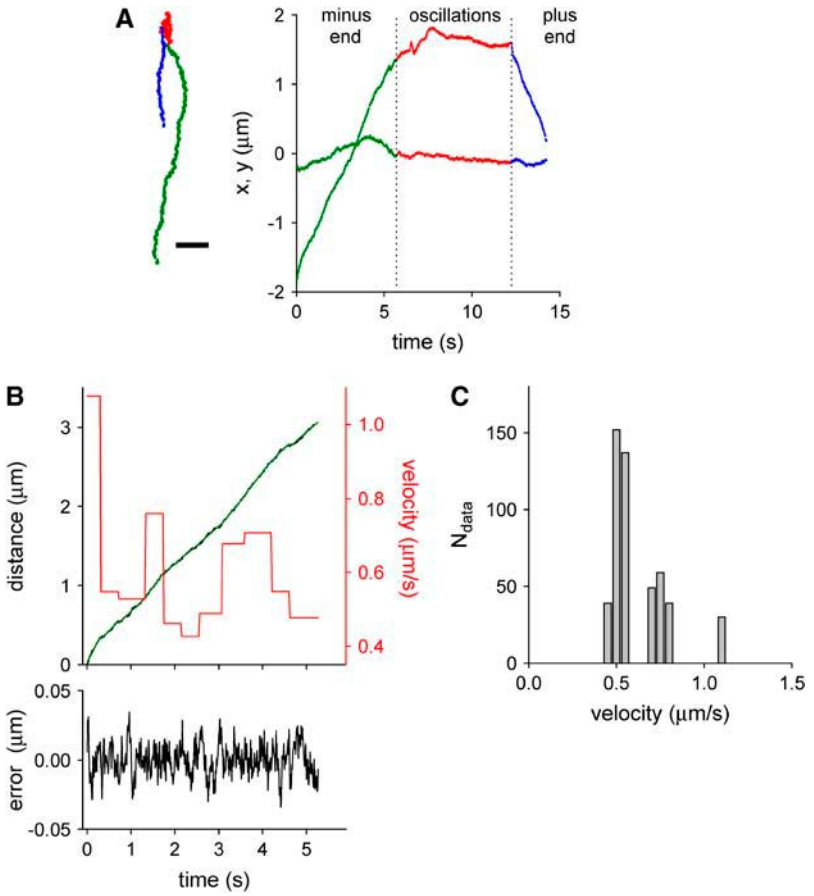

FIGURE 1 Determination of local velocities. The trajectory and individual coordinates obtained for the melanosome were classified under minus-end run (*green*), plus-end run (*blue*), or oscillations in position (*red*) according to the criteria described (scale bar, 0.5 μm). (*A*). The fragment corresponding to the minus-end run (*black line*) was divided into segments of 40 points and a linear equation was fitted to each of these segments (*green line*). From the slope of the best-fitting equation, the velocities were obtained for each of the segments (*red*). The bottom part of *B* shows the residuals obtained from the fitting. The velocity data were binned and included in the corresponding histogram (*C*).

This was confirmed by tracking melanosomes in cells fixed with 4% formaldehyde (not shown).

Velocity distribution of melanosomes during aggregation

Melanophores were incubated for 30 min at room temperature in serum-free medium in the presence of 10 μM latrunculin B to depolymerize the actin filaments. The movement of the melanosomes was induced by addition of melatonin from a 10-μM stock in ethanol to a final concentration of 10 nM. After incubating the cells with melatonin for 5 min, we recorded 10–20 movies per cell, from which we determined an average of 100 melanosome trajectories. All the recordings were made with cells incubated in melatonin for 5–15 min. As an example, the inset to Fig. 3 shows the first frame of a movie overlapped with the trajectory of one of the melanosomes. In this particular case, the cell nucleus was located at the top left of the frame. Since the minus ends of the microtubules are attached to the centrosome, which is located near the nucleus, we can conclude that the melanosome depicted in the figure was moving toward the minus end of the microtubule.

Fig. 3 shows the distance traveled by the same melanosome as a function of time. As can be observed from the plot, the velocity—i.e., the slope of the curve—remains approximately constant for long periods of time, indicating that there is a constant force driving the transport of the melanosome during these intervals. To quantitatively analyze the velocity in the trajectories, we divided each trajectory into segments of at least 40 data points (i.e., 0.4 s) and fit a linear equation from which we calculated the average velocity in each segment (for details in the procedure for segmentation of the trajectories, see Materials and Methods). We did not consider those segments in which the fitting was not satisfactory or if the velocity was lower than 100 nm/s. This value was the minimum velocity measured for melanosomes presenting a defined directional motion.

We classified the segments of constant velocity according to whether they were moving toward or away from the nucleus and constructed velocity histograms for these two sets of data. As mentioned before, the motion toward the nucleus is mainly due to melanosomes moving in the minus-end direction by the action of cytoplasmic dynein, whereas the motion away from the nucleus is due to melanosomes moving toward the plus end of microtubules by the action of kinesin-2.

Fig. 4 *A* shows the velocity histogram obtained in one of the cells for melanosomes moving in the minus-end direction. We tried to fit the histograms corresponding to melanosomes moving in the minus- or plus-end directions

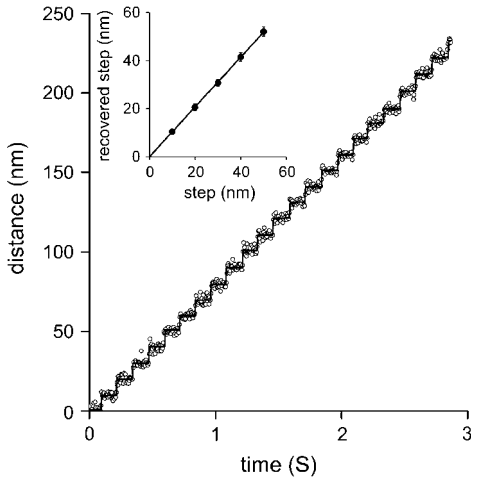

FIGURE 2 Tracking performance. A nanometric stage placed on top of the microscope was programmed to move a slide containing a dried suspension of microspheres in steps of 10–50 nm. Movies of the beads were registered as described in Materials and Methods at 200 frames/s and the particle trajectories were obtained by using the pattern-recognition algorithm. The trajectory of one of the beads moving in steps of 10 nm is plotted as a function of time. (*Inset*) Size of the step obtained by analyzing the particles trajectories as a function of the input step.

with single Gaussian distribution functions, since this would be the distribution expected for a homogeneous population of motors moving a cargo (21). However, the experimental distributions present clear deviations from this function, suggesting that a more complex distribution function is required to satisfactorily fit the experimental data.

Also, we determined that 63% of the data points correspond to melanosomes driven in the minus-end direction,

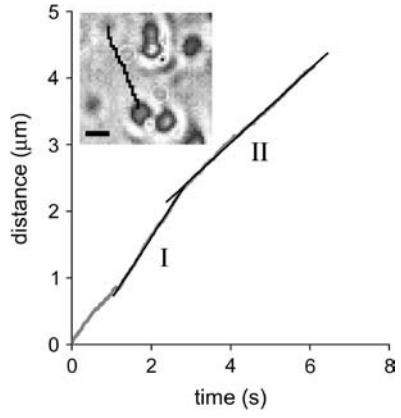

FIGURE 3 Tracking melanosomes in cells. The distance traveled by one of the melanosomes in a cell stimulated with melatonin was measured as described in the text and is represented as a function of time. The continuous lines represent the fit of a linear equation in two regions of the trajectories. From the fitting, we calculated the following velocities in the segments: 0.922 ± 0.003 (*I*) and 0.551 ± 0.001 (*II*) μm/s. (*Inset*) Initial frame of a movie recorded for the same cell at 100 frames/s. The melanosomes appears in the image as black circles. The trajectory of the chosen melanosome is overlapped with the image (*black line*). (Scale bar,1 μm.)

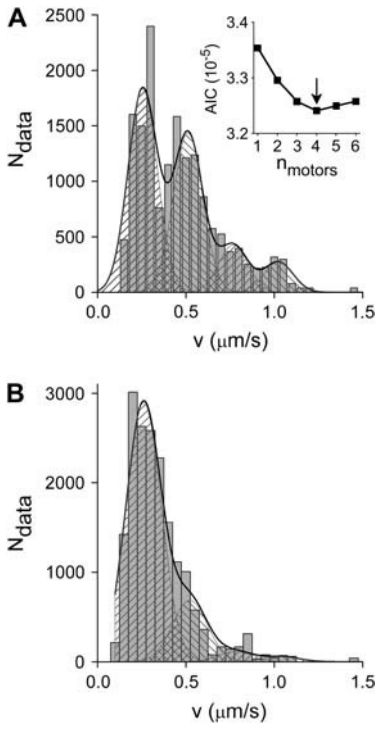

FIGURE 4 Distribution of velocities of melanosomes. Movies of different regions of two cells stimulated for aggregation (*A*) or dispersion (*B*) were recorded as described and the organelle trajectories and velocities calculated. The histograms of velocities were constructed from data of melanosomes moving toward the minus (*A*) or plus (*B*) ends of the microtubules. The continuous lines correspond to the fitting of Eq. 5 with the following best-fitting parameters: $v_1 = 0.250 \pm 0.009$ μm/s, $\sigma = 0.078 \pm 0.006$ μm, $A_1 = 1520 \pm 240$, $A_2 = 1230 \pm 220$, $A_3 = 360 \pm 140$, and $A_4 = 240 \pm 140$ *(A)*; and $v_1 = 0.260 \pm 0.007$ μm/s, $\sigma = 0.098 \pm 0.007$ μm/s, $A_1 = 000 \pm 300$, $A_2 = 700 \pm 140$, $A_3 = 115 \pm 113$, and $A_4 = 60 \pm 100$ *(B)*. The gray lines show the contribution of each peak to the total distributions. The inset to *A* shows the AIC values calculated by fitting Eq. 5 to the histogram considering *n* values from 1 to 6.

reflecting a lower relative contribution of kinesin-2 to melanosome transport after melatonin treatment.

Distribution of melanosome velocity during dispersion

To study the motion of melanosomes during dispersion, we treated the cells as described above, with the exception that we added 100 nM MSH instead of melatonin. Movies of the cells were recorded and analyzed as described in the previous section. As was verified for the aggregation process, the experimental velocity distribution of minus- and plus-end directed melanosomes could not be correctly fit by single Gaussian distribution functions (Fig. 4 *B*). The percentage of melanosomes moving toward the minus end after MSH stimulation was 32%, indicating a lower relative contribution of dynein to melanosome transport during dispersion and demonstrating that movement of melanosomes along microtubules is regulated even in the absence of contribution from actin and myosin-V.

Melanosome motion along EGFP-labeled microtubules

To determine if the modulation of melanosome velocity is due to changes in the number of microtubule tracks used by the melanosomes, we followed the motion of the melanosomes in melanophores in which the microtubules were labeled by EGFP-tagged XTP, a *Xenopus* homolog of mammalian microtubule-associated protein tau (18). This approach allowed us to follow the motion of melanosomes and to register the microtubule tracks along which the melanosomes are moving. Fig. 5, *A* and *C*, shows fluorescence images of labeled cells treated with latrunculin and melatonin obtained under two-photon excitation. It can be observed that the microtubules presented a highly homogeneous staining; we consider that those cytoskeleton tracks presenting a higher intensity represent two or more microtubules very close to each other, whereas those tracks with lowest intensity correspond to single microtubules.

As can also be observed from the figures, we could detect bright spherical particles. By overlapping the fluorescence and the brightfield images, we determined that those particles are melanosomes (Fig. 6). It has not been described previously that *Xenopus* melanosomes are fluorescent under two-photon excitation; we are currently working to understand the source of the light emission.

Since the melanosomes are easily detected by two-photon microscopy, we followed their motion by using a routine designed to track fluorescent particles (19). In this way, we do not have to switch between brightfield and fluorescence mode, hence the lag time between the image acquisition and the tracking is minimized.

Fig. 5, *A* and *C*, also shows the trajectories of two melanosomes overlaid on the fluorescence images obtained before the tracking. We analyzed the melanosome velocities in regions of the trajectories (delimited by *arrows* in the figures) in which the melanosomes were moving toward the center of the cell along a single microtubule. Fig. 5, *B* and *D*, shows the distance traveled by these melanosomes as a function of time. As the data obtained in a single trajectory is not enough to construct a velocity histogram, we arbitrarily divided the trajectories in segments of variable size and fitted the data within the segments to linear equations to determine if there are changes in velocity through the selected region of the trajectory. The legend to the figure indicates the velocity values recovered in these segments and the r^2 value obtained for the regression in each case. It can be observed that the velocity varies suddenly during the run of the melanosomes along single microtubules, indicating that the changes in velocity are not related to changes in the number of microtubules interacting with an organelle.

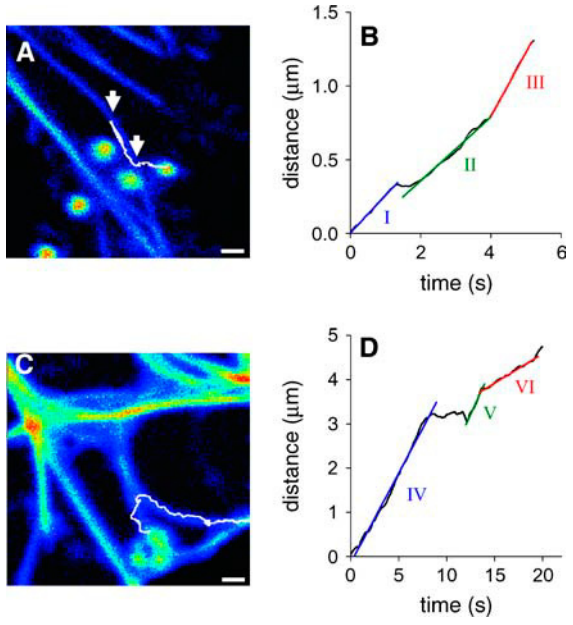

FIGURE 5 Tracking melanosomes moving along a single microtubule. Cells with microtubules labeled with EGFP-XTP were treated with latrunculin B and stimulated for pigment aggregation with melatonin. Two-photon fluorescence images of the cells were taken (excitation wavelength = 915 nm) and the melanosomes, detected as bright spots in these images, were tracked as described above. (*A* and *C*) The trajectories recovered for two of the melanosomes moving toward the minus end of the microtubules are superimposed over the fluorescence images taken for the cells. Scale bar, 1 μm. The distance traveled by the melanosomes in different regions of these trajectories (*arrows*) was plotted as a function of time (*B* and *D*, respectively). The continuous lines show the fitting of a linear equation to different segments of the trajectories. The velocities (in nm/s) and r^2 values were 255 ± 2, 0.9988 (*I*); 216 ± 3, 0.9936 (*II*); 438 ± 3, 0.9993 (*III*); 406 ± 2, 0.9963 (*IV*); 480 ± 7, 0.9941 (*V*); and 132 ± 1, 0.9959 (*VI*).

A model for melanosome transport in cells

In the previous sections, we observed that the velocity histograms of melanosomes transported by cytoplasmic dynein or kinesin-2 present complex distributions. Moreover, in some of the trajectories we observed sudden transitions in the velocity of transport toward both the minus and the plus ends of microtubules, indicating a change in the force responsible for the melanosome motion.

The simplest model that could explain these results is to consider that the melanosomes are transported by a variable

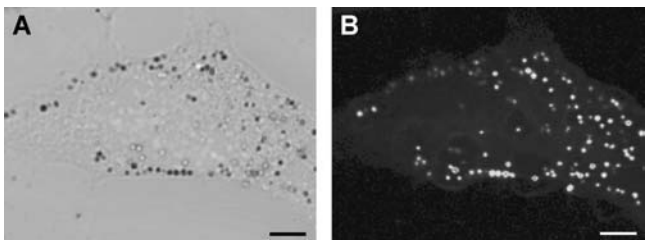

FIGURE 6 Imaging melanophores. Comparison between brightfield (*A*) and two-photon excitation fluorescence (*B*) images of a melanophore revealed that melanosomes are observed under two-photon excitation. The excitation wavelength was 780 nm. (Scale bars, 5 μm).

number of copies of the motor molecule. If each of the motor molecules contributes equally to the transport, the velocity of the melanosome (v_i) is related to the number of motors (n_i) as follows:

$$v_i = \frac{n_i F_{motor}}{\alpha}, \quad (4)$$

where F_{motor} is the force exerted by a single molecular motor, and α is the friction coefficient. This equation is similar to that proposed by Grill et al. (22).

According to this model, the velocity histogram of melanosomes transported by a given motor will present peaks located at integer multiples of the velocity corresponding to a melanosome transported by a single copy of the motor (v_1). If we consider that each peak presents a Gaussian distribution,

$$N = \sum_{n_i-1}^{n} A_i e^{-\frac{(v-v_1 n_i)^2}{2\sigma^2}}, \quad (5)$$

where N is the number of data points with velocity v, A_i is the amplitude of the peak corresponding to melanosomes transported by n_i motors, and σ is the half-width of the peaks.

In this equation, we consider the same width for all the peaks, since this parameter mainly depends on the intracellular motion, which increases the noise in the velocity determination, the size distribution of the melanosomes, and the viscosity variations in the cell cytoplasm.

The model was fit to the histograms obtained for individual cells during aggregation or dispersion considering n values between 1 and 6. We verified that the best fit of the histograms is obtained with $n = 4$, indicating that each melanosome moving in the minus or plus direction is transported by four or fewer active motors. The continuous line in Fig. 4 shows the fitting of the model.

The v_1 and σ values calculated for kinesin-2 by fitting Eq. 5 to the histograms of the observed cells were 280 ± 60 nm/s and 120 ± 40 μm/s during aggregation and 240 ± 65 nm/s and 100 ± 20 nm/s during dispersion. In the case of cytoplasmic dynein, the calculated v_1 and σ were 260 ± 50 nm/s and 100 ± 25 nm/s during aggregation and 240 ± 30 nm/s and 90 ± 25 nm/s during dispersion. The errors in v_1 and σ were calculated as the standard deviations of the parameter values determined in the different cells. It can be observed that the velocity of melanosomes transported by one dynein molecule is not significantly different from the velocity of those transported by one kinesin-2. Also, the values of v_1 measured for each motor during aggregation and dispersion are similar, considering the error in v_1 determination.

Our model is based on the observation of peaks located at regular intervals in the histograms of melanosome velocity. However, this can result from errors due to the finite sampling of a unimodal distribution. To test if this is the case, we applied a statistical autocorrelation method proposed by Stratford et al. (23) to study whether the peaks obtained in synaptic amplitude frequency histograms result from a quantal distribution.

In this method, the test histogram is smoothed using a fast Fourier transform (FFT) filter to obtain a unimodal distribution in which individual peaks are eliminated. The difference function between the histogram and the unimodal distribution is lightly smoothed by FFT filtering and its autocorrelation function is computed. An autocorrelation score (AC) is calculated as the difference between the value of the first peak and that of the first valley of the autocorrelation functions. This score depends on the sharpness of the histogram peaks, the equality of their spacing, and the number of data. Hence, it is related to the probability that the test histogram arises from a multimodal distribution. The spacing between the peaks can be obtained from the period of the autocorrelation function.

Fig. 7 shows the results obtained from this analysis applied to the histogram of dynein-driven melanosomes in a cell stimulated for aggregation. The autocorrelation function shows a characteristic ''damped sinusoid'' shape expected for a multimodal distribution. The first peak is located at ~250 nm/s, with subsequent peaks occurring approximately every 250 nm/s. This result agrees with the peak periodicity obtained from the proposed model.

We also run control simulations in which we applied the autocorrelation analysis to histograms generated from random velocity data. The distribution of these simulated data followed a unimodal Weibull function the parameter values of which were obtained by fitting this function to the experimentally determined test histogram (for details of the simulation procedure, see Stratford et al. (23)). Then, we performed the autocorrelation analysis in these simulated histograms using the same FFT filters used for the test histograms. The correlation plot of these histograms did not

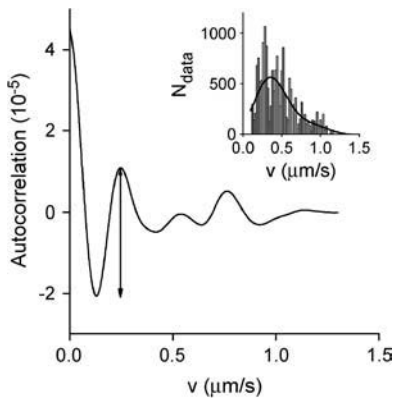

FIGURE 7 Autocorrelation analysis. A histogram of dynein-driven melanosomes obtained after stimulating the cells for aggregation was finely binned and filtered as described in the text until a unimodal curve (inset) was obtained. The difference function resulting from subtraction of the unimodal curve from the histogram was lightly smoothed, and the autocorrelation of the smoothed difference function was calculated. The arrow points the valley and peak used to calculate the AC score.

show oscillatory behavior (not shown). The AC scores of the simulated histograms were 20-fold lower than the experimental AC score ($N = 5$), indicating that the experimental histograms do not arise from a unimodal distribution.

To quantify the contribution to the transport of melanosomes with a different number of active motors, we constructed histograms for dynein- and kinesin-2-driven melanosomes by adding the individual histograms obtained for each cell. As there are small variations from cell to cell in the velocity of the melanosomes attached to a single copy of the motor, we divided the velocity in each histogram by v_1 and added the normalized histograms of the different cells. We fit to the histograms obtained for dynein or kinesin-driven melanosomes a normalized distribution equation:

$$N = \sum_i A_i \, e^{-\frac{\left(\frac{v}{v_1} - n_i\right)^2}{2\sigma'^2}}. \quad (6)$$

Fig. 8 represents the amplitude of the peaks relative to the amplitude measured for the peak corresponding to melanosomes attached to one active motor. These values are directly related to the probability of finding a melanosome dragged by n_i motors. It can be observed that the melanosomes are transported in the minus-end direction mainly by the action of one or two active dynein motors, with a lower probability of three or four motors contributing to the movement. The figure also shows that the relative number of melanosomes moved by more than one dynein is higher during aggregation. In the case of kinesin-2, the transport toward the plus end of the microtubules is mainly due to melanosomes bound to one or two active motors and has the same characteristics during aggregation and dispersion.

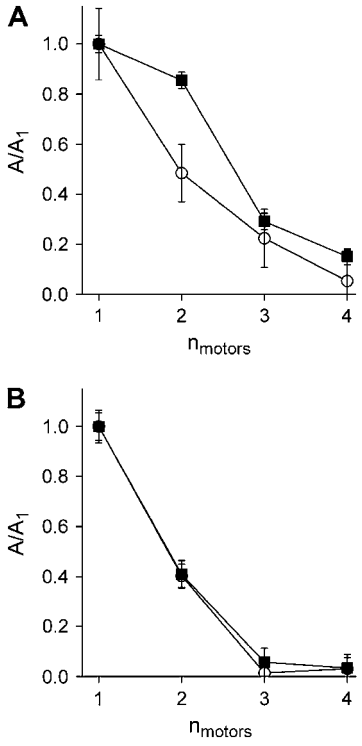

FIGURE 8 Relative population of melanosomes attached to a different number of active motors. The relative amplitude of the peaks in the normalized histograms corresponding to melanosomes attached to dynein (*A*) and kinesin-2 (*B*) motors is represented as a function of the number of active motors during aggregation (*solid symbols*) and dispersion (*open symbols*).

DISCUSSION

In this article, we studied the properties of organelle transport in live cells employing a new fast-tracking method. We used pigment cells for this study because the pigment organelles can be tracked with a high S/N ratio. In addition, pigment organelle transport can be biased toward the plus or minus ends of microtubules by treating the cells with MSH or melatonin, respectively, allowing us to analyze the regulation of organelle transport.

To have a precise description of melanosome motion, we designed a new method for fast imaging and accurate tracking of particles, which uses an inverted microscope under wide-field illumination. As melanosomes are black and relatively big organelles, they can be easily detected in these conditions. The high natural contrast of melanosomes allows us to improve the image acquisition rate and the precision of the tracking with respect to previous works in which the organelle tracking required labeling with a fluorescent probe and observation with, for example, a confocal scanning microscope. In these conditions, the rate of movie acquisition is on the order of one image per second (2).

The tracking method used in this work does not require the assumption of an intensity distribution function for the particle; instead, it uses the particle's own intensity profile to determine its position as a function of time. This approach enhances the precision when tracking particles such as melanosomes in which the intensity cannot be fit with a Gaussian distribution function.

The main limitation of the method used in this work is that the tracking is in two dimensions. However, as we are measuring transport along microtubules and they are radially distributed in the cell and mainly extended parallel to the cell surface we would expect the motion in the z direction to be considerably less than in the x,y plane.

The experimental approach described previously allowed us to measure the velocity distribution of melanosomes moving along microtubules by the action of cytoplasmic dynein and kinesin-2 motors after stimulating the cells for either aggregation or dispersion. We eliminated the contribution of transport along actin filaments by treating the cells with latrunculin B, which binds to actin monomer, resulting in depolymerization of actin filaments (24).

As mentioned above, we would expect melanosome velocities to follow a single Gaussian distribution function if each of these organelles is transported by a single copy of a motor protein. However, the experimental velocity

histograms of either kinesin-2- or dynein-driven melanosomes could not be fit by such a distribution function. In fact, the histograms presented multiple peaks distant from each other in regular velocity intervals, suggesting that a more complex process is responsible for the motion of melanosomes in vivo.

One possible explanation to the observed distributions is that the differences in the melanosome velocity are mainly due to variations of the viscosity of the cell cytoplasm. However, these variations are expected to be continuous (25), and therefore they cannot be the cause of the discrete distributions observed in Fig. 4. Also, several authors explored the viscoelasticity of the cytoplasm of different cell lines using vesicles or beads similar in size to the melanosomes (see, for example, Bausch et al. (25) and Hill et al. (26)) and found viscosity values at least 1000 times higher than the water viscosity. Using this kind of probes, Bausch et al. (25) determined that there are not significant differences in the viscoelastic properties through the cytoplasm. Extrapolating these results to melanophores, the high viscosity of the cytoplasm results in a viscous drag sufficient to slow down the melanosomes.

Recently, it has been shown that cytoplasmic dynein decrease the step size in response to an increasing load (27). This gear mechanism could contribute in vivo to regulate the velocity of the motor. However, the step size of dynein in *Drosophila* S2 cells is constant and equal to 8 nm, indicating that the motor is working at high load (9) and suggesting that the gear mechanism is not responsible for the velocity distribution observed in this work for dynein.

A simple model to explain our experimental results is that there are different melanosome populations, which are transported by a different number of copies of the given motor protein. The binding of organelles to microtubules by the action of more than one motor protein, has been suggested by Ashkin et al. (28), who observed by electron microscopy that mitochondria of 320-nm diameter have 1–4 molecular cross-bridges to microtubules in the giant amoeba *Reticulomyxa*. Welte et al. (29) observed that the force driving lipid droplets in *Drosophila* embryos changes during development in a quantized fashion and proposed that this phenomenon is due to variations in the number of active motors. More recently, Kural et al. (9) have demonstrated that up to 11 kinesins or dyneins work together during the transport of peroxisomes in *Drosophila* S2 cells, moving the cargo more quickly than one motor could by itself.

Hunt et al. (30) assayed the motion of microtubules of different lengths moving across high-density kinesin-coated glass surfaces through a medium of viscosity similar to that of the cytoplasm. In this case, the number of motors bound to the microtubule increases in proportion to the microtubule length. They found that the microtubule speeds were independent of their lengths, indicating that all the active motors bound to the microtubule contribute equally to its transport. Taking this data into account, we presume that a single melanosome would double its velocity if the number of active motors moving it doubles (Eq. 4).

As seen in Figs. 4 and 6, the model proposed in this work could explain the experimental velocity distributions of melanosomes in vivo. Our results demonstrate that the active motion of melanosomes in melanophores is regulated at the level of a single organelle. We found that the velocity distribution of melanosomes moving toward the cell center changes depending on the state of the cell. In contrast, the movement of melanosomes away from the center has the same properties in the presence of signals for aggregation and dispersion. If our model is correct, this result implies that the average number of active dynein motors transporting a melanosome increases during aggregation, whereas the number of kinesin-2 molecules does not change. These data agree very well with our earlier results (17), which showed that only the minus-end component of the microtubule-dependent transport is regulated, whereas the plus-end component is constitutively active.

Taking into account the results shown in Fig. 8 and the velocity of the organelles carried by single copies of either dynein or kinesin-2 (v_1 values), we determined the average velocity for minus- and plus-end-directed melanosomes during aggregation and dispersion. These values agree with the mean velocities previously reported for melanosomes moving in similar conditions (17).

Gross et al. (17) demonstrated that the stimulation with melatonin increases the run length (''processivity'') of minus-end directed melanosome movement along microtubules. According to our results, this phenomenon can be explained by an increase in the number of active motors moving the organelle. The transport powered by multiple motors would be more processive since the probability of detaching the motor from the microtubule will decrease with an increase in the number of active motors (2). Therefore, the increase of the average number of active dynein motors will increase the run length.

It is worth mentioning that the direct measurement of dynein and kinesin-2 contents on the surface of melanosomes did not show any measurable differences between organelles purified from cells undergoing aggregation and dispersion (17), suggesting that the increase in the number of active motors transporting the melanosome does not result from an increased binding of the motor to the melanosome surface. Therefore, one can suggest that cytoplasmic dynein is activated or inhibited without ever dissociating from the organelle. The molecular mechanism involved in this activation may include structural modifications of the motor itself, changes in the associated proteins such as the dynactin complex, or a redistribution of dynein in the organelle membrane.

Two different mechanisms have been postulated to explain the unidirectional transport of vesicles attached simultaneously to two opposing motors. In the first model, the motors are involved in a tug-of-war with the stronger

motor determining the direction of motion at any particular moment. In the second model, the motors are coordinated, so that when the melanosome moves in one direction, the opposing motors are inactive (31).

The performance of dynein in kinesin-2 dominant negative melanophores did not improve with respect to wild-type melanophores (17), suggesting that cytoplasmic dynein and kinesin-2 are not involved in the tug-of-war with each other (for detailed analysis of the possible mechanisms of motor coordination during transport of melanosomes and other organelles see Welte (2) and Gross (31)). Our results also agree with the coordination model since the positions of the peaks observed in the velocity histogram of melanosomes attached to either dynein or kinesin-2 are the same during aggregation and dispersion. This result indicates that no matter how many copies of the motor of one polarity move an organelle in one direction, this movement is not counteracted by the motor of opposite polarity.

This research was supported by the Division of Research Resources of the National Institutes of Health (PHS 5 P41-RR03155), by a grant from the National Institute of General Medical Sciences to V.I.G. (GM-52111), and by the University of Illinois at Urbana-Champaign.

REFERENCES

1. Howard, J. 2001. Structures of motor proteins. *In* Mechanics of Motor Proteins and the Cytoskeleton. Sinauer Associates, Sunderland, MA. 197–212.
2. Welte, M. A. 2004. Bidirectional transport along microtubules. *Curr. Biol.* 14:R525–R537.
3. Vale, R. D. 2003. The molecular motor toolbox for intracellular transport. *Cell.* 112:467–480.
4. Yildiz, A., J. N. Forkey, S. A. McKinney, T. Ha, Y. E. Goldman, and P. R. Selvin. 2003. Myosin V walks hand-over-hand: single fluorophore imaging with 1.5-nm localization. *Science.* 300:2061–2065.
5. Yildiz, A., H. Park, D. Safer, Z. Yang, L. Q. Chen, P. R. Selvin, and H. L. Sweeney. 2004. Myosin VI steps via a hand-over-hand mechanism with its lever arm undergoing fluctuations when attached to actin. *J. Biol. Chem.* 279:37223–37226.
6. Yildiz, A., M. Tomishige, R. D. Vale, and P. R. Selvin. 2004. Kinesin walks hand-over-hand. *Science.* 303:676–678.
7. Schnitzer, M. J., K. Visscher, and S. M. Block. 2000. Force production by single kinesin motors. *Nat. Cell Biol.* 2:718–723.
8. Mallik, R., and S. P. Gross. 2004. Molecular motors: strategies to get along. *Curr. Biol.* 14:R971–R982.
9. Kural, C., H. Kim, S. Syed, G. Goshima, V. I. Gelfand, and P. R. Selvin. 2005. Kinesin and dynein move a peroxisome in vivo: a tug-of-war or coordinated movement? *Science.* 308:1469–1472.
10. Nascimento, A. A., J. T. Roland, and V. I. Gelfand. 2003. Pigment cells: a model for the study of organelle transport. *Annu. Rev. Cell Dev. Biol.* 19:469–491.
11. Rozdzial, M. M., and L. T. Haimo. 1986. Bidirectional pigment granule movements of melanophores are regulated by protein phosphorylation and dephosphorylation. *Cell.* 47:1061–1070.
12. Sammak, P. J., S. R. Adams, A. T. Harootunian, M. Schliwa, and R. Y. Tsien. 1992. Intracellular cyclic AMP not calcium, determines the direction of vesicle movement in melanophores: direct measurement by fluorescence ratio imaging. *J. Cell Biol.* 117:57–72.
13. Tuma, M. C., A. Zill, N. Le Bot, I. Vernos, and V. Gelfand. 1998. Heterotrimeric kinesin II is the microtubule motor protein responsible for pigment dispersion in *Xenopus* melanophores. *J. Cell Biol.* 143:1547–1558.
14. Rogers, S. L., and V. I. Gelfand. 1998. Myosin cooperates with microtubule motors during organelle transport in melanophores. *Curr. Biol.* 8:161–164.
15. Nilsson, H., and M. Wallin. 1997. Evidence for several roles of dynein in pigment transport in melanophores. *Cell Motil. Cytoskeleton.* 38:397–409.
16. Rogers, S. L., I. S. Tint, P. C. Fanapour, and V. I. Gelfand. 1997. Regulated bidirectional motility of melanophore pigment granules along microtubules in vitro. *Proc. Natl. Acad. Sci. USA.* 94:3720–3725.
17. Gross, S. P., M. C. Tuma, S. W. Deacon, A. S. Serpinskaya, A. R. Reilein, and V. I. Gelfand. 2002. Interactions and regulation of molecular motors in *Xenopus* melanophores. *J. Cell Biol.* 156:855–865.
18. Olesen, O. F., H. Kawabata-Fukui, K. Yoshizato, and N. Noro. 2002. Molecular cloning of XTP, a tau-like microtubule-associated protein from *Xenopus laevis* tadpoles. *Gene.* 283:299–309.
19. Levi, V., Q. Ruan, and E. Gratton. 2005. 3-D particle tracking in a two photon microscope. application to the study of molecular dynamics in cells. *Biophys. J.* 88:2919–2928.
20. Akaike, H. 1974. A new look at the statistical model identification. *IEEE Trans. Automat. Control.* 19:716–723.
21. Badoual, M., F. Julicher, and J. Prost. 2002. Bidirectional cooperative motion of molecular motors. *Proc. Natl. Acad. Sci. USA.* 99:6696–6701.
22. Grill, S. W., J. Howard, E. Schaffer, E. H. Stelzer, and A. A. Hyman. 2003. The distribution of active force generators controls mitotic spindle position. *Science.* 301:518–521.
23. Stratford, K. J., J. J. Jack, and A. U. Larkman. 1997. Calibration of an autocorrelation-based method for determining amplitude histogram reliability and quantal size. *J. Physiol.* 505:425–442.
24. Spector, I., N. R. Shochet, D. Blasberger, and Y. Kashman. 1989. Latrunculins—novel marine macrolides that disrupt microfilament organization and affect cell growth: I. Comparison with cytochalasin D. *Cell Motil. Cytoskel.* 13:127–144.
25. Bausch, A. R., W. Moller, and E. Sackmann. 1999. Measurement of local viscoelasticity and forces in living cells by magnetic tweezers. *Biophys. J.* 76:573–579.
26. Hill, D. B., M. J. Plaza, K. Bonin, and G. Holzwarth. 2004. Fast vesicle transport in PC12 neurites: velocities and forces. *Eur. Biophys. J.* 33:623–632.
27. Mallik, R., B. C. Carter, S. A. Lex, S. J. King, and S. P. Gross. 2004. Cytoplasmic dynein functions as a gear in response to load. *Nature.* 427:649–652.
28. Ashkin, A., K. Schutze, J. M. Dziedzic, U. Euteneuer, and M. Schliwa. 1990. Force generation of organelle transport measured in vivo by an infrared laser trap. *Nature.* 348:346–348.
29. Welte, M. A., S. P. Gross, M. Postner, S. M. Block, and E. F. Wieschaus. 1998. Developmental regulation of vesicle transport in *Drosophila* embryos: forces and kinetics. *Cell.* 92:547–557.
30. Hunt, A. J., F. Gittes, and J. Howard. 1994. The force exerted by a single kinesin molecule against a viscous load. *Biophys. J.* 67:766–781.
31. Gross, S. P. 2003. Dynactin: coordinating motors with opposite inclinations. *Curr. Biol.* 13:R320–R322.